

## INFLUENCE OF MILLING PARAMETERS ON PARTICLE SIZE AND MICROHARDNESS OF CRYOMILLED AND SPARK PLASMA SINTERED CP Ti

KOZLÍK Jiří<sup>1</sup>, BECKER Hanka<sup>2</sup>, STRÁSKÝ Josef<sup>1</sup>, HARCUBA Petr<sup>1</sup>, JANEČEK Miloš<sup>1</sup>

<sup>1</sup>Charles University in Prague, Department of Physics of Materials, Prague, Czech Republic, EU

[Jiri.Kozlik@seznam.cz](mailto:Jiri.Kozlik@seznam.cz)

<sup>2</sup>TU Bergakademie Freiberg, Institute of Materials Science, Freiberg, Germany, EU

### Abstract

Ultra-fine grained (UFG) materials are in the spotlight because of their enhanced mechanical properties. UFG material can be prepared by bottom-up process consisting of agglomeration of nano-particles or by top-down process of severe plastic deformation (SPD). In this study, Ti Grade 2 powder underwent attritor milling in liquid nitrogen (LN) and argon (LAr) and was consequently consolidated via spark plasma sintering (SPS). The influence of milling liquid (LN vs. LAr), of milling balls material (stainless steel vs. tungsten carbide) and of other milling parameters (e.g. speed, duration) on size and shape of powder particles, chemical contamination and microhardness was investigated. Particle size reduction was generally not observed, while their morphology changed significantly due to simultaneous disintegration and intensive cold welding during the milling process. Using LN as a cooling medium resulted in very high nitrogen content (up to 3 wt.%), and consequent embrittlement and hardening with microhardness values attaining 800 HV. LAr seems to be more suitable for milling of titanium, but a process control agent (stearic acid) must be added to prevent excessive cold welding. Microhardness of material without nitrogen contamination rose from original 178 HV to 200-300 HV range, depending on milling efficiency.

**Keywords:** Titanium, cryomilling, spark plasma sintering, contamination, microhardness

### 1. INTRODUCTION

Severe plastic deformation (SPD) is well known to strengthen materials via reducing the grain size and increasing dislocation density [1]. Ultra-fine grained commercially pure Ti (CP Ti) has been already prepared by high pressure torsion [2, 3] and equal-channel angular pressing [4] and an improvement of mechanical properties was demonstrated. More recently, powder metallurgy methods are becoming more popular, especially in the perspective of near-net shape processing [5].

A wide palette of materials has been already prepared by cryogenic ball milling (cryomilling) [6], incl. CP Ti. It has been observed that particles repeatedly collide among themselves and balls, are disintegrated and cold-welded together again. The balance these two processes determines final particle size. Every particle is also repetitively plastically deformed, while the cryogenic temperature suppresses recovery and grain growth of the material. For CP Ti, crystallite size of approx. 20 nm was reported [7, 8, 9]. Enhanced strength was also observed for compact material after consolidation via isostatic forging or spark plasma sintering (SPS) [9, 10, 11]. Both liquid nitrogen (LN) and liquid argon (LAr) were used for cooling, but only steel balls as a milling medium.

Spark plasma sintering is a novel promising method for powder consolidation. The sintered material is pressed in a die, while being internally heated by Joule heat due to pulse direct electric current passing through [12]. Physical processes occurring during SPS are not fully understood yet, but all experiments show that material can be sintered in much shorter times and lower temperatures when compared to conventional techniques (e.g. [12]). These are desirable processing conditions, because they suppress grain growth during the sintering process retaining fine grained structure.

The main goal of this paper is an investigation of influence of a cooling liquid, balls material, process control agent and process parameters (e.g. milling speed and duration) on particle size and morphology, chemical contamination and microhardness of cryomilled and spark plasma sintered CP Ti.

## 2. EXPERIMENTAL METHODS

Commercially pure Ti Grade 2 powder was prepared by gas atomization and supplied by TLS Technik GmbH & Co. Spezialpulver KG (Germany). Chemical composition as claimed by the manufacturer is shown in **Table 1**. The powder was stored and handled in air.

**Table 1** Chemical composition of as-received powder as claimed by supplier

| Element        | Ti      | Fe   | O    | H     | C     | N     |
|----------------|---------|------|------|-------|-------|-------|
| Content (wt.%) | balance | 0.08 | 0.14 | 0.001 | 0.006 | 0.004 |

### 2.1. Sample preparation

The milling process was performed in the Union Process 01-HD attritor (1400 cm<sup>3</sup>) with liquid nitrogen (LN) or liquid argon (LAr) as a cooling agent. As grinding media, two different materials of balls were used - 440C stainless steel (SS) and tungsten carbide in cobalt matrix (WC-Co). In both cases the ball diameter was 6.35 mm (1/4 in). Because the density of WC-Co (15.6 g/cm<sup>3</sup>) is approx. twice as high as the density of SS, ball-to-powder ratio (BPR) is also doubled, while the volume of balls and weight of powder feed was identical. An overview of performed milling with process parameters can be seen in **Table 2**. When milling with heavier WC-Co balls, speed had to be adjusted to avoid motor overload and intended milling time of 4 hours could not be achieved due to the higher consumption of limited amount of LN.

**Table 2** An overview of milling process parameters

| Sample label   | Cooling agent | Balls used | BPR | Milling time (h:min) | Rotation speed | Stearic acid (g) |
|----------------|---------------|------------|-----|----------------------|----------------|------------------|
| 4/700-N-SS     | LN            | SS         | 16  | 4:00                 | 700            | -                |
| 3/650-N-WC     | LN            | WC-Co      | 31  | 3:15                 | 650            | -                |
| 4/700-Ar-SS    | LAr           | SS         | 16  | 4:00                 | 700            | -                |
| 8/700-Ar-SS    | LAr           | SS         | 16  | 8:00                 | 700            | -                |
| 4/700-Ar-SS-SA | LAr           | SS         | 16  | 4:00                 | 700            | 15               |
| 4/350-Ar-SS-SA | LAr           | SS         | 16  | 4:00                 | 350            | 15               |

To prevent cold welding during milling, a stearic acid (SA) was used as a process control agent in the amount of 15 g (0.5 wt.% of total balls and powder weight). Since the residuals of SA presented during sintering process could result in an unwanted contamination, milled powders were repeatedly washed in acetone and filtered, causing SA to be dissolved from particle surface. Powders were then dried under vacuum.

The sintering procedure was performed in vacuum in a SPS device HDP 25 produced by FCT Systeme GmbH (Germany) using graphite die, cylindrical samples with a diameter of 20 mm and 5 mm in height. The actual sintering process consisted of heating at the rate of 100 K / min to the 600 °C temperature, followed by 1 min dwell accompanied by an increase of mechanical pressure on the piston to 80 MPa. After that, heating continued to 750 °C. At this temperature, the isothermal sintering was performed for 3 min. Subsequent cooling was not controlled, approximate initial rate was about 200 K / min and decreased at lower temperatures.

## 2.2. Microstructure investigations

All samples were investigated on the cross-section. For particle analysis, powders were hot mounted in synthetic resin, ground and polished using SiC papers, 3  $\mu\text{m}$  diamond suspension and OP-S with  $\text{H}_2\text{O}_2$  and diluted  $\text{HNO}_3$  and HF. For microstructure and microhardness analysis, sintered samples were cut, ground and polished using SiC papers, 3  $\mu\text{m}$  and 1  $\mu\text{m}$  diamond suspensions and 0.25  $\mu\text{m}$  alumina suspension.

Images of both powder and sintered samples were taken using scanning electron microscope FEI Quanta 200F (FEG). The chemical composition (and contamination from milling) was determined by EDX and carrier hot gas extraction (CHGE) analysis, CHGE method for N, O and H contents.

Microhardness measurements were performed on Qness Q10A automatic microhardness testing machine using Vickers method with the load of 0.5 kg and 10 s dwell time.

## 3. RESULTS AND DISCUSSION

### 3.1. Particle size and morphology

Particles size and shape were determined from low magnification SEM images (not shown) and described by their *equivalent diameter* (a diameter of a thought circle with the same area as the observed cross-section of the particle) and *elongation* (a ratio of max. and min. Feret's diameter [13]), respectively. Observed area fractions were plotted against *equivalent diameter* and *elongation* are shown in the **Figure 1 a)** and **b)**, respectively. Lognormal distribution was fitted to the *equivalent diameter data to calculate*, particle mean size and its standard deviation (**Table 3**). Comparison of particle morphology is shown in the **Figure 2**.

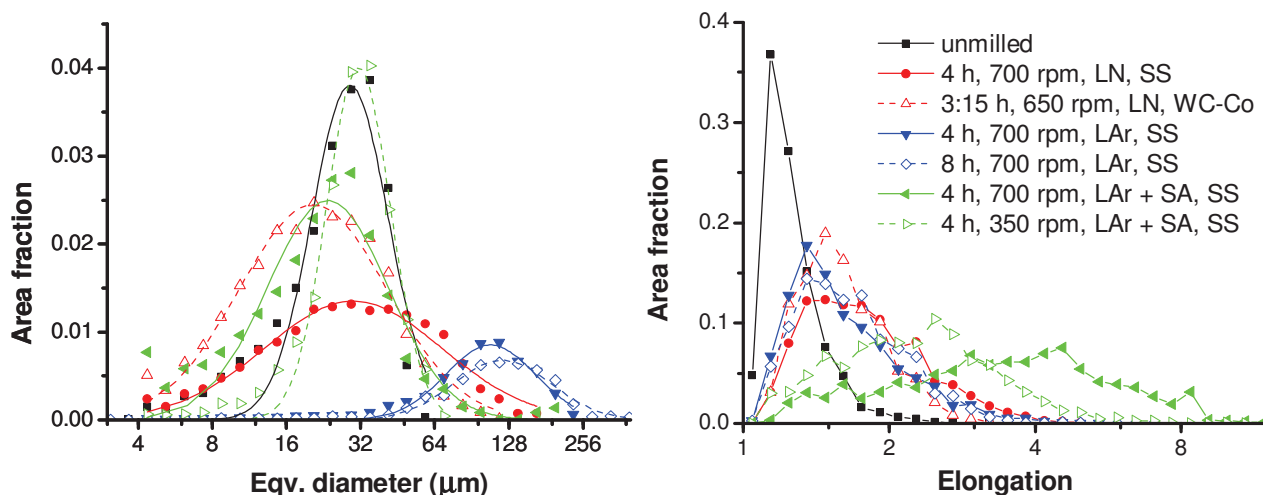


**Figure 1** a) particle size (*equivalent diameter*) b) *elongation* distributions. The legend is common for both graphs. In a), fitted lognormal distributions are shown, while in b) the lines are guides for an eye

**Table 3** Mean particle size of powders and its standard deviation (for sample labels see **Table 2**)

| Sample                               | Unmilled    | 4/700-N-SS  | 3/650-N-WC  | 4/700-Ar-SS  | 8/700-Ar-SS  | 4/700-Ar-SS-SA | 4/350-Ar-SS-SA |
|--------------------------------------|-------------|-------------|-------------|--------------|--------------|----------------|----------------|
| Particle mean size ( $\mu\text{m}$ ) | $35 \pm 13$ | $83 \pm 83$ | $42 \pm 33$ | $140 \pm 62$ | $165 \pm 80$ | $37 \pm 24$    | $36 \pm 11$    |

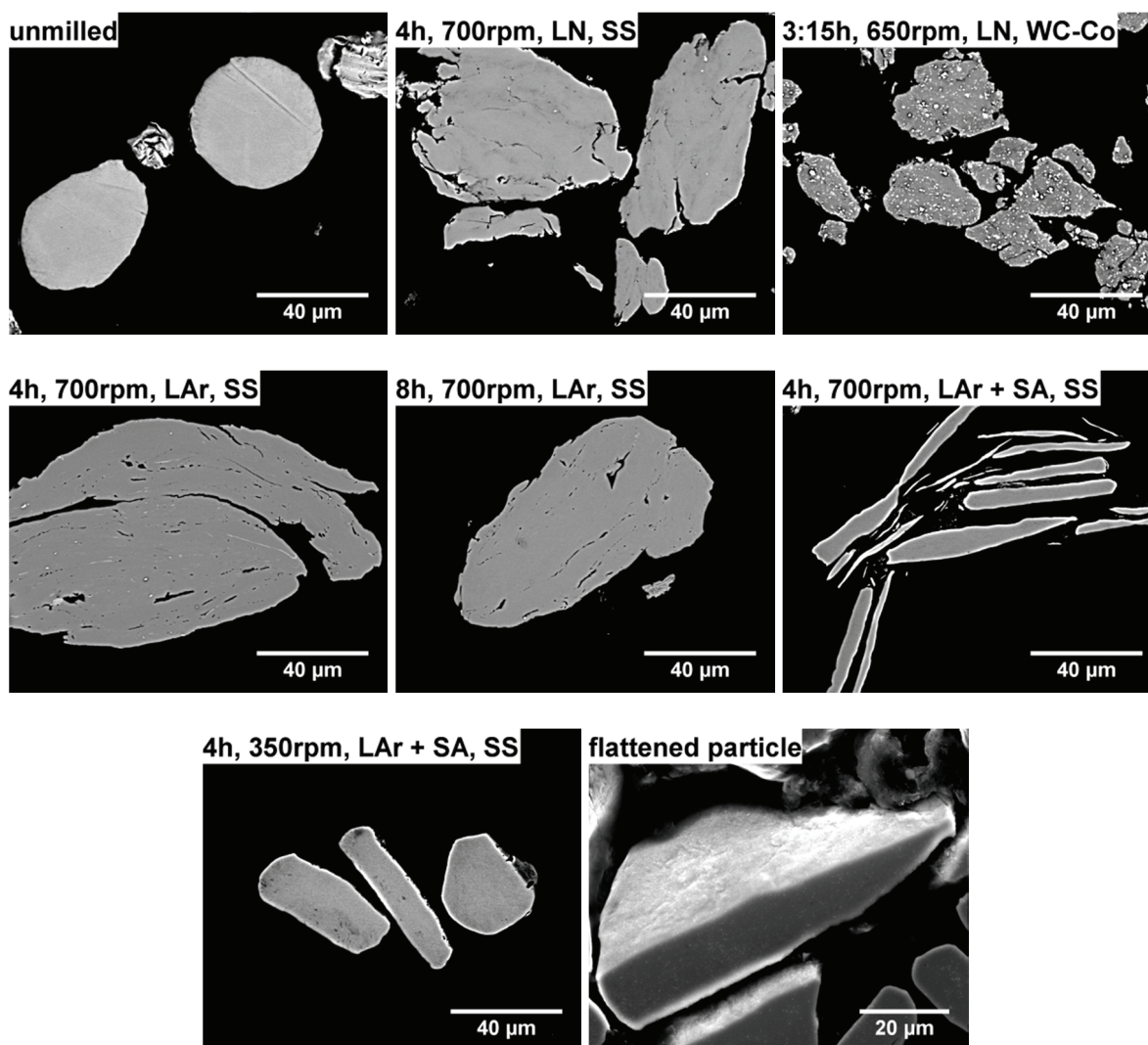


**Figure 2** SEM micrographs of typically sized and shaped particles. The last image shows that particles milled with SA are flattened, not rod-shaped as could be guessed from the cross-section images.

Unmilled (gas atomized) particles are almost perfectly round. During milling in LAr without application of process control agent (stearic acid), powder particles have strong tendency to be cold-welded together, which results in increased mean size. Layered structure of cold-welded particles can be seen in the **Figure 2** (4 and 8 h in LAr without SA). Balls and milling chamber were also completely covered with a layer of cold-welded Ti.

Using LN as a cooling liquid also shows cold-welded particles, but it results in smaller overall mean size than in the case of LAr. This can be attributed to increased brittleness caused by high nitrogen content (as will be discussed later). Milling with WC-Co balls is also much more efficient than with SS balls, since mean particle size is approximately halved.

Particle mean size remains almost unchanged, after milling in LAr with stearic acid (SA), which suggests that cold-welding is effectively suppressed by SA and individual particles are only deformed. Particles are elongated on the cross section, their true shape is a flake or a plate. This is shown in **Figure 2** (flattened particle), where a whole particle is visible, and also supported by [14]. Particle size distribution of powder milled at lower speed of 350 rpm is similar to that of unmilled powder. In the case of powder milled at 700 rpm, smaller particles are more frequently observed and the size distribution is broader, therefore the initial particles are not only deformed, but also disintegrated.

### 3.2. Contamination

Chemical contamination during milling is an inevitable problem. The likely sources are these: the cooling liquid, grinding balls, the milling tank, stearic acid and manipulation in air. Beside the gas contamination measured by CGHE (**Table 4**), Fe and WC-Co contamination was measured by the EDX on powder samples. Fe content was  $(0.35 \pm 0.05)$  wt.% and independent on milling parameters. In the WC-Co milled powder,  $(4.09 \pm 0.04)$  wt.% of W and  $(0.97 \pm 0.02)$  wt.% of Co was detected. We assume that WC-Co balls became partly brittle under low temperatures and fragments were incorporated into the Ti particles (which can be seen in the **Figure 2** as bright spots inside the particles). Increase of C content was detected only in the sample milled with WC-Co balls. Quantitative analysis was not done due to the low sensitivity of EDX to C.

**Table 4** Contamination of powders and sintered samples by O, N and H (estimated relative error 5 %)

|                | O content (wt.%) |          | N content (wt.%) |          | H content (wt.%) |          |
|----------------|------------------|----------|------------------|----------|------------------|----------|
|                | powder           | sintered | powder           | sintered | powder           | sintered |
| Unmilled       | 0.16             | 0.17     | 0.02             | -        | <0.001           | -        |
| 4/700-N-SS     | 0.43             | 0.40     | 0.80             | 0.83     | <0.001           | -        |
| 3/650-N-WC     | 0.38             | 0.39     | 2.99             | 2.98     | <0.001           | -        |
| 4/700-Ar-SS    | 0.23             | 0.25     | 0.20             | 0.20     | <0.001           | -        |
| 8/700-Ar-SS    | -                | 0.26     | -                | 0.20     | -                | -        |
| 4/700-Ar-SS-SA | 0.36             | 0.37     | 0.06             | 0.06     | 0.05             | 0.02     |
| 4/350-Ar-SS-SA | 0.48             | 0.21     | 0.03             | 0.01     | 0.30             | 0.01     |

The nitrogen content is several times higher in powders milled in LN than in LAr, especially when WC-Co balls are used. The major source of the nitrogen contamination is therefore liquid nitrogen (not nitrogen in air). Furthermore, more severe deformation by WC-Co balls leading to smaller particles further enhances nitrogen content. It also appears that SA is able to reduce the nitrogen content (possibly by creating a protective film on the particle surface), while the amount of hydrogen and oxygen increases (which is caused by the SA itself). In the case of the sample 4/350-Ar-SS-SA, cleaning of powder in acetone was not sufficient, which resulted in significantly higher H content.

### 3.3. Microhardness

**Table 5** summarizes the microhardness measurements. Milling in LN leads to very hard material, which is unfortunately also very brittle which was demonstrated by cracks at indent corners (not shown). The HV 0.5 values after milling in LN can be fully attributed to the strengthening by interstitial N atoms [15].

**Table 5** Microhardness (HV 0.5) of sintered samples (for sample labels see **Table 2**).

| Sample                               | Unmilled    | 4/700-N-SS   | 3/650-N-WC   | 4/700-Ar-SS  | 8/700-Ar-SS  | 4/700-Ar-SS-SA | 4/350-Ar-SS-SA |
|--------------------------------------|-------------|--------------|--------------|--------------|--------------|----------------|----------------|
| Particle mean size ( $\mu\text{m}$ ) | $178 \pm 6$ | $487 \pm 25$ | $834 \pm 55$ | $243 \pm 17$ | $261 \pm 21$ | $245 \pm 12$   | $199 \pm 5$    |

In the case of LAr milled powders, hardness maximum was achieved after 8 hours of milling, when induced deformation is the highest. Significantly higher HV values ( $\sim 350$  HV) reported in [10] achieved under slightly different milling conditions (8 h, 180 rpm, BPR 30:1) can be fully attributed to higher N content ( $\sim 0.6$  wt.%). There does not seem to be any difference between milling with or without SA in the terms of hardness. Lower hardness of the sample milled at 350 rpm can originate either from lower milling energy, or it can be the result of insufficiently cleaned SA, which impeded the sintering process. Solid solution hardening model described

in [15] cannot be applied quantitatively, since it assumes a homogenous distribution of interstitials and bulk material (with no porosity).

#### 4. CONCLUSIONS

CP Ti Grade 2 was prepared by cryogenic milling and spark plasma sintering under different milling conditions. We can conclude following:

- Particle size is not generally reduced by cryomilling, Particles are repetitively disintegrated and cold welded. However, if PCA is used, only individual particles are deformed leading to particle size reduction.
- Particle morphology is changed significantly and particle elongation rises with increasing energy of milling.
- Milling in LN leads to very high N content, which results in high hardness and brittleness. SA utilization reduces the nitrogen contamination. Careful cleaning can also reduce H and O content. WC-Co balls become partly brittle and are the source of extra contamination.
- Cryomilling increases material hardness. Further investigations should be performed to distinguish between contamination and grain refinement hardening mechanisms.

#### ACKNOWLEDGEMENTS

***Czech Science Foundation project 15-15609S is gratefully acknowledged.***

#### REFERENCES

- [1] ZHILYAEV, A. P., LANGDON, T. G. Using high-pressure torsion for metal processing: fundamentals and applications. *Prog. Mater. Sci.*, 2008, vol. 53, no. 6, pp. 893-979.
- [2] POPOV, A. A., PYSHMINTSEY, I. Y., DEMA KOV, S. L., ILLARIONOV, A. G., LOWE, T. C., SERGEYEVA, A. V., VALIEV, R. Z., Structural and mechanical properties of nanocrystalline titanium processed by severe plastic deformation. *Scr. Mater.* 1997, vol. 37, no. 7, pp. 1089-1094.
- [3] JANEČEK, M., STRÁSKÝ, J., ČÍŽEK, J. et al. Mechanical properties and dislocation structure evolution in Ti6Al7Nb alloy processed by high pressure torsion. *Metall. Mater. Trans. A*, 2014, vol. 45, no. 1, pp. 7-15.
- [4] VALIEV, R.Z. Structure and mechanical properties of ultrafine-grained metals. *Mater. Sci. Eng. A*, 1997, vol. 234-236, pp. 59-66.
- [5] QIAN, M., FROES, F. H. *Titanium Powder Metallurgy*. 1<sup>st</sup> ed. Boston: Butterworth-Heinemann, 2015, 648 p.
- [6] WITKIN, D. B., LAVERNIA, E. J. Synthesis and mechanical behavior of nanostructured materials via cryomilling. *Prog. Mater. Sci.*, 2006, vol. 51, no. 1, pp. 1-60.
- [7] SUN, F., ROJAS, P., ZÚÑIGA, A., LAVERNIA, E. J. Nanostructure in a Ti alloy processed using a cryomilling technique. *Mater. Sci. Eng. A*, 2006, vol. 430, no. 1-2, pp. 90-97.
- [8] DHEDA, S., MELNYK, C., MOHAMED, F. A. Effect of titanium nitride nanoparticles on grain size stabilization and consolidation of cryomilled titanium. *Mater. Sci. Eng. A.*, 2013, vol. 584, pp. 88-96.
- [9] ERTORER, O., TOPPING, T., LI, Y., MOSS, W., LAVERNIA, E. J. Enhanced tensile strength and high ductility in cryomilled commercially pure titanium. *Scr. Mater.*, 2009, vol. 60, no. 7, pp. 586-589.
- [10] ERTORER, O., ZÚÑIGA, A., TOPPING, T., LI, Y., MOSS, W., LAVERNIA, E. J. Mechanical behavior of cryomilled CP-Ti consolidated via Quasi-Isostatic forging. *Met. Mat. Trans. A.*, 2009, vol. 40, no. 1, pp. 91-103.
- [11] ERTORER, O., TOPPING, T. D., LI, Y., MOSS, W., LAVERNIA, E. J. Nanostructured Ti Consolidated via Spark Plasma Sintering. *Metall. Mater. Trans. A*, 2011, vol. 42, no. 4, pp. 964-973.
- [12] GUILLON, O., GONZALEZ-JULIAN, J., DARGATZ, B. et al. Field-assisted sintering technology/spark plasma sintering: Mechanisms, materials, and technology developments. *Adv. Eng. Mater.*, 2014, vol. 16, no. 7, pp. 830-849.
- [13] <https://imagej.nih.gov/ij/docs/guide/146-30.html>
- [14] SURYANARAYANA, C. Mechanical alloying and milling. *Prog. Mater. Sci.*, 2001, vol. 46, no. 1-2, pp. 1-184.
- [15] OGDEN, H. R. JAFFEE, R. I., Effects of carbon, oxygen, and nitrogen on mechanical properties of titanium and titanium alloys. *TML Report (20)*, Titanium Metallurgical Laboratory, Battelle Memorial Institute, Columbus, Ohio, 1955.